Electronic Supplementary Material (ESI) for Journal of Materials Chemistry C.
This journal is © The Royal Society of Chemistry 2024

Electronic Supplementary Material for

Discrete and Dimeric Chiral Plasmonic Nanorods: Intrinsic Chirality and Extrinsic Chirality

Weiwei Fu, ‡[a, b] Jiaqi Chen, ‡[c] Shunping Zhang, [a, d] Guangchao Zheng, *[a, b] Yuan Zhang*[a, b]

[a]*School of Physics and Microelectronics, Key laboratory of Material Physics, Ministry of Education, Zhengzhou University, Zhengzhou, 450001, China*

[b]*Institute of Quantum Materials and Physics, Henan Academy of Sciences, Zhengzhou 450046, China*

[c]*School of Mechanical Engineering, Chengdu University, Chengdu 610000, China*

[d]*Center for Nanoscience and Nanotechnology, and School of Physics and Technology, Wuhan University, Wuhan 430072, China*

1 Experimental Section

1.1 Chemicals

Chloroauric acid ($HAuCl_4 \cdot 3H_2O$, ≥99.9%), silver nitrate ($AgNO_3$, ≥99.0%), N-Hexadecyltrimethylammonium Chloride (CTAC, ≥99.0%), Hexadecyl trimethyl ammonium bromide (CTAB, ≥99.0%), Sodium borohydride ($NaBH_4$, ≥98.0%), L-Ascorbic acid (AA, ≥99.0%), hydrochloric acid (HCl, ≥37.0%), L-Cysteine (L-Cys, ≥97.0%), D-Cysteine (D-Cys, ≥97.0%), glutathione (GSH, ≥98.0%), 4-aminothiophenol (4-ATP, ≥98.0%). All these chemicals are purchased from Adamas. DI water (18.25 MΩ.cm).

1.2 Instruments

The PCD measurements were recorded with J-810 spectrophotometer (JASCO, Japan). The extinction spectra were carried out by the UV-1900 (SHIMADZU). Transmission electron microscopy (TEM, JEM-2010, 200 kV). A commercial finite element analysis software, COMSOL Multiphysics 5.4, was used to perform the calculations.

1.3 Synthesis of Au NRs

1.3.1 Seeds preparation

Firstly, 250 μL of $HAuCl_4$ solution with a concentration of 0.01 M was mixed with 10 mL of CTAB with a concentration of 0.1 M, and then 600 μL of $NaBH_4$ solution with a concentration of 0.01 M was added to the solution. The solution turned from golden yellow to light brown. Grow for 2~2.5 hours in a 30 ℃ electric blast drying oven.

1.3.2 Growth steps

40 mL of 0.1M CTAB solution was mixed with 2 mL of 0.01 M $HAuCl_4$ solution, and then 400 μL of 0.01 M $AgNO_3$ solution was added to the mixed solution. After mixing, 320 μL of 0.1 M AA was added. After mixing the solution evenly from golden color colorless transparent solution. Finally, 800 μL of 1 M HCl solution and 96 μL of seed solution were added. Shake evenly and put in 30 ℃ electric blast drying oven overnight growth. Finally, the solution changed from colorless to purplish red.

1.4 Synthesis of dc-Au NRs

The Au NRs solution was centrifuged twice (8000 rpm for 5 min) and then dispersed in the CTAB solution. 1 mL Au NRs solution was added into 3 mL 10 mM CTAB, then 150 μL 2 mM L-Cys (D-Cys), and finally 20 μL 10 mM 4-ATP. The solution was then put into an electric blast drying oven at 30 ℃ for reaction for 3 hours. The reaction solution was successively added with 35 μL of 10 mM $AgNO_3$, 65 μL of 10 mM $HAuCl_4$, and 28 μL of 0.1 M AA, and then put into an electric heating air drying oven at 70 ℃ for 1 hour. After synthesis, the dc-Au NRs were centrifuged at 6500 rpm for 5 min twice to remove supernatant for TEM.

1.5 Synthesis of dc-Au NRs Dimers

The dc-Au NRs were centrifuged once (6500 rpm for 5 min) and filled with deionized water. Then add 100 μL of 10 mM GSH and adjust pH to 3.0 with 1 M HCl, then put into an electric heating air drying oven at 45 ℃ for 12 hours. After synthesis, the dc-Au NRs dimers were centrifuged at 6500 rpm for 5 min twice to remove supernatant for TEM.

2 Supplementary Figures

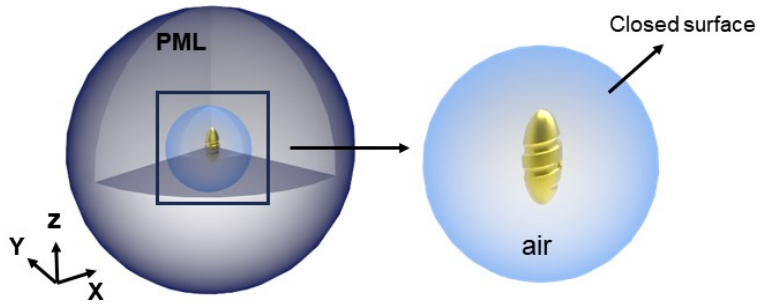

Fig. S1 Construction of simulation model for dc-Au NRs.

The scattering/absorption/extinction cross-sections, near-field distributions were calculated by using the commercial COMSOL software. The dc-Au NRs simulation model was set according to the geometrical parameters obtained from the TEM images and 3D reconstruction data. As shown in Figure S1, the dc-Au NR has a length of 57.5 nm and half-axis of 20 nm along the short axis, respectively, and the chiral feature on the surface has a radius of 15 nm and a helical depth about 10 nm. The dc-Au NR is placed inside a spherical computational domain with a radius of 200 nm, that is capped by a 300 nm thick shell for the perfectly matched layer. The geometric center of the dimer is aligned with the origin of coordinates. The incident light propagates along the z-axis from the positive to the negative direction. The refractive index of the surrounding medium is 1. The scattered light, containing both the components of left- and right-handed circularly polarized light, is collected by a closed surface S surrounding the dc-Au NR with a radius of 200 nm. The simulation is performed under y-polarized light, left- and right-handed circularly polarized light. The wavelength range is from 400 nm to 900 nm.

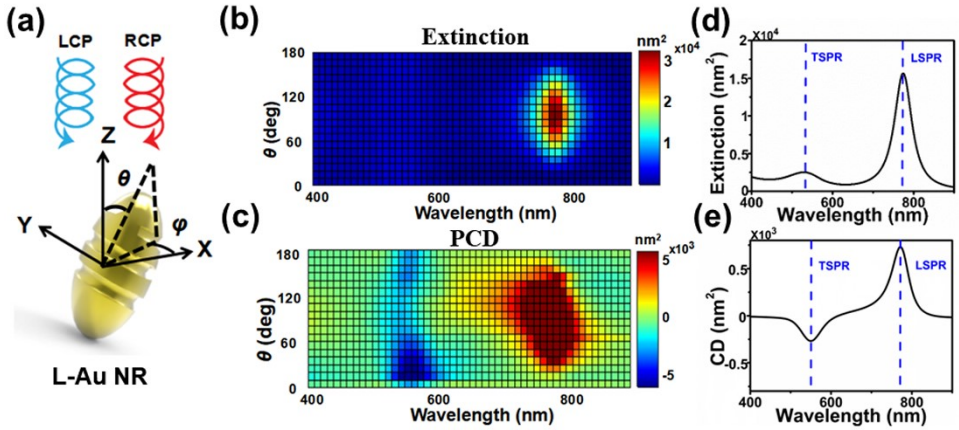

Fig. S2 Influence of orientation of L-Au NR to the light incidence on the PCD response. (a) Schematic of the incident left-/right-polarized light along the negative z-axis, and the dc-Au NRs with orientation specified by the polar angle θ and azimuth angle φ. The NRs have a length of 57.5 nm and half-axis of 20 nm along the short axis, respectively, and the chiral feature on the surface has a radius of 15 nm and a helical depth about 10 nm. (b, c) Calculated extinction (b) and PCD (c) spectra for $\theta = 0^o,10^o,20^o,\cdots 180^o$ and given $\varphi = 0^o$. The results for given θ do not show significant dependence on the angle φ. (d, e) Calculated extinction (d) and PCD (e) spectra by integrating the spectra for the angle $\theta = 0^o,\cdots 180^o$, $\varphi = 0^o,\cdots 360^o$, which resemble the experimental results shown in Fig. 1c and d.

In Fig. S2, we show the results similar to those in Fig. 2 of the main text but for the L-Au NR. These results are similar except that the PCD spectra in Fig. S2c is a mirror of those in Fig. 2c with respect to the x-axis.

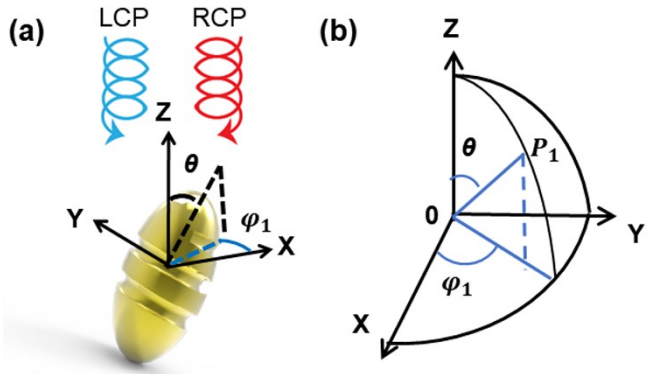

Fig. S3 Schematic diagram of phi at different azimuth angles. (a) Schematic diagram of dc-Au NR under light incidence;（b） schematic diagram of phi angle in spherical coordinates.

In Fig. S3, we represent the dc-Au NR as a line segment OP, which can be determined by two angles (θ, φ) at any position in space. Here, θ is the positive angle between the line segment OP and the z-axis, and φ is the angle rotated counterclockwise from the x-axis to the OP from the positive z-axis. While keeping the θ angle constant and changing the φ angle, the projection of the line segment OP on the x-y plane remains constant.

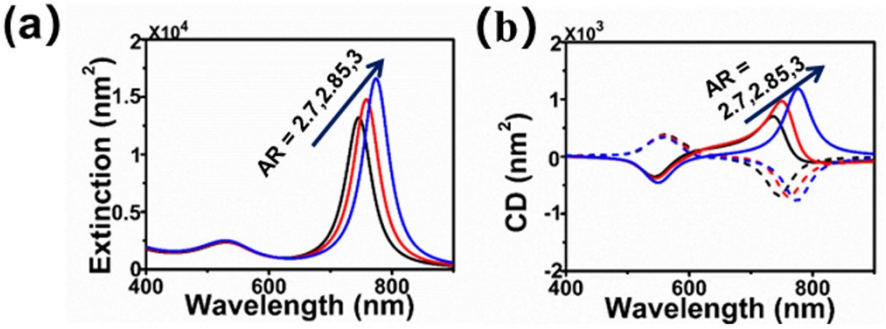

Fig. S4 Extinction (a) and PCD (b) spectra of dc-Au NRs with increasing aspect ratio (AR) = 2.7, 2.85, 3 (black, red and blue lines). The solid and dashed lines represent the NRs with left- and right-handed surfaces.

In Fig. S4, we show the extinction spectra (a) and PCD spectra (b) for chiral NRs with increasing aspect ratio. As this ratio increases, the TSPR has only a slight increase in intensity, while the LSPR has a significant red-shift and increased intensity. By averaging these spectra, we will be able to reproduce the broad spectra measured in the experiment, highlighting the influence of the inhomogeneity of dc-Au NRs.

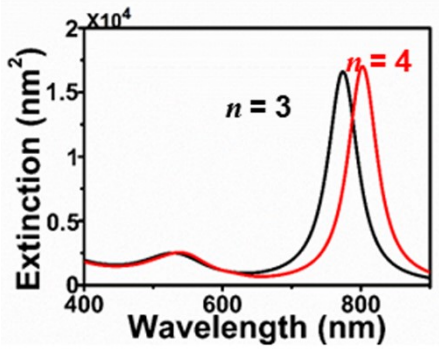

Fig. S5 Calculated PCD for *d* = 10 nm, *w* =30 nm and increasing *n* = 3, 4 (red and black lines).

Fig. S5 shows that by increasing the turning number *n* of the helical pitches, we observed a slight red-shift in the extinction spectra.

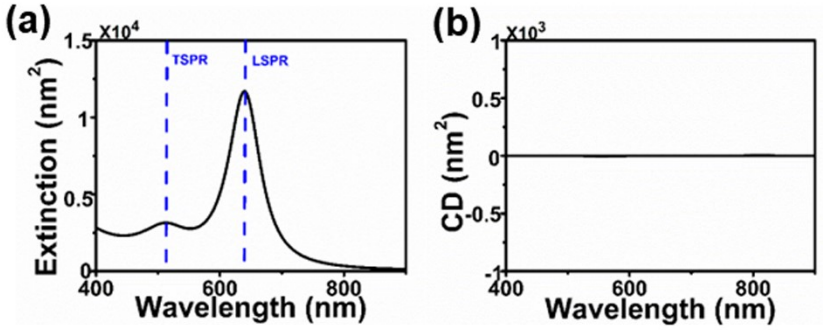

Fig. S6 Extinction (a) and PCD (b) spectra of an achiral Au NR.

In Fig. S6, we show the extinction (a) and PCD (b) spectra of an achiral Au NR with smooth surface. The extinction spectra resemble those of dc-Au NRs, except that the peaks due to LSPR appear at much shorter wavelength, highlighting the influence of chiral feature on the wavelength of LSPR as examined in Fig. 3 of the main text. The PCD spectra of the achiral Au NRs show no obvious chiral feature, verifying that the PCD response of the dc-Au NRs originates from the chiral feature on the metal surfaces.

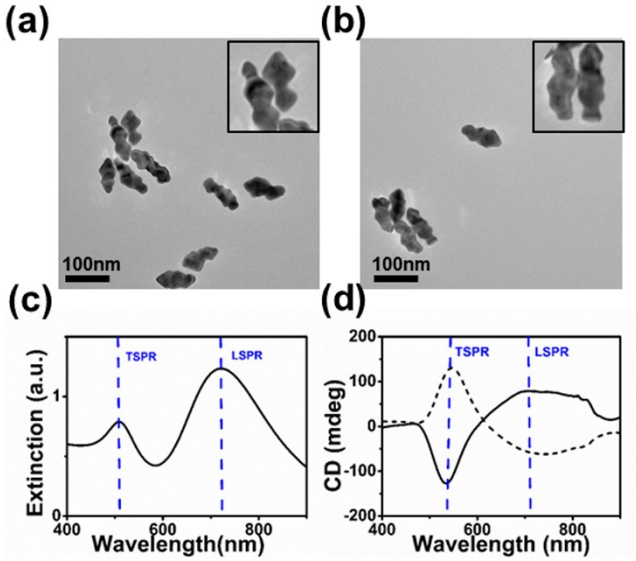

Fig. S7 Experimental results for dimers of dc-Au NRs. (a, b) show the exemplary TEM images of dc-Au NRs dimers synthesized in the experiment. (c, d) show the corresponding extinction spectra and PCD spectra.

In Fig. S7, we show two sets of different TEM images (a, b) with the enlarged part (insets), which show clearly the dc-Au NRs dimer and provide the experimental support for our theoretical simulation of dc-Au NRs dimer in the main text. Fig S7c and d show the corresponding extinction spectra and PCD spectra, where both TSPR and LSPR showed significant blue-shift relative to dc-Au NRs (Fig. 1c and d).

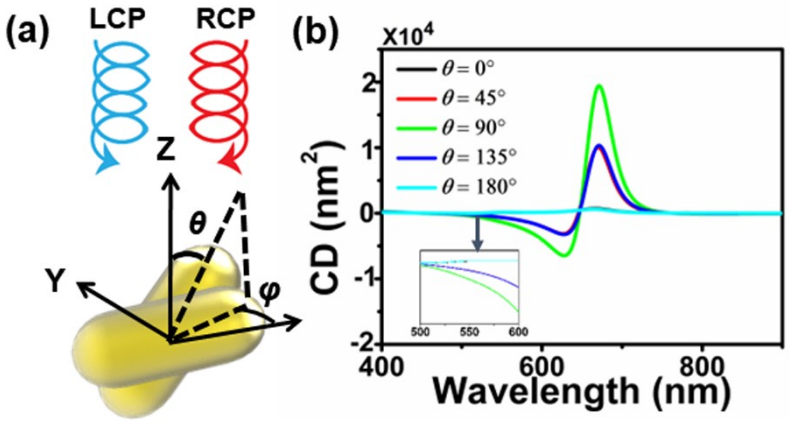

Fig. S8 Influence of different incident direction illumination condition on the PCD response of self-assembled achiral Au NRs. (a) Schematic of the incident left-/right-polarized light along the negative z-axis, and two identical intersected achiral Au NRs with orientation specified by the polar angle θ and azimuth angle φ. (b) Calculated PCD spectra for $\theta = 0^o$,45^o,...180^o and given $\varphi = 90^o$.

In Fig. S8, we show PCD spectra for self-assembled achiral Au NRs with separation 80 nm at different angles θ and given $\varphi = 90^o$. It can be found that at $\theta = 0^o$ or $\theta = 180^o$, the PCD has almost no signal, while at other angles, the PCD spectra show obvious extrinsic chirality, which are similar to the results of the Fig.4b in the main text, it proves that structural chirality dominates.

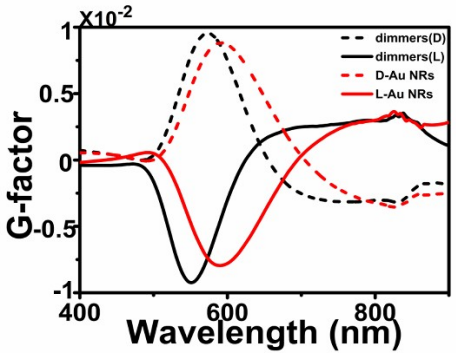

Fig. S9 Comparison of self-assembled dc-Au NRs and dc-Au NRs g-factors.

In Fig. S9, we studied the g-factor of the self-assembled dc-Au NRs (black curves) and the dc-Au NR (red curves) firstly. We found that the g-factor for former was slightly larger, indicating the possible coupling between the nanoparticles enhance their chiroptical response.

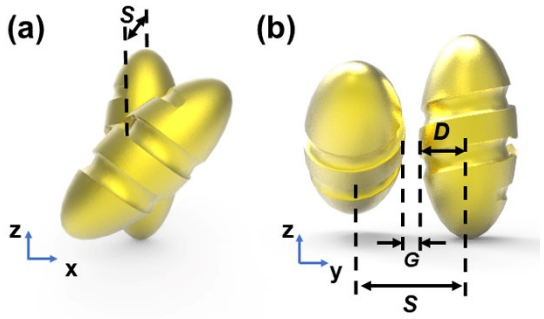

Fig. S10 Diagram of center distance *S* and gap distance *G*. (a) self-assembled dc-Au NRs in the x-z direction. (b) self-assembled dc-Au NRs in the y-z direction.

Fig. S10 illustrates a schematic representation of the self-assembled dc-Au NRs in different planes. The distance *S* refers to the center-center distance between two nanorods, and the actual gap distance between the two dc-Au NRs is *G*, which can be achieved by subtracting two times of the short-axis radius *D*, *G = S-2*D*.

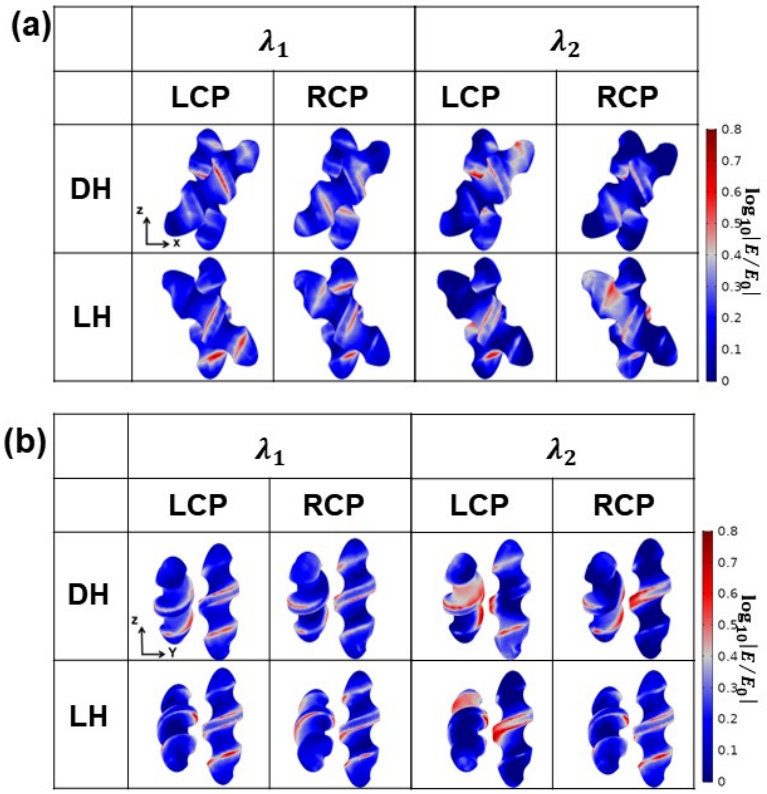

Fig. S11 Electric field enhancement distribution around the self-assembled dc-Au NRs. (a) show the field intensity distribution of wavelength λ_1 and wavelength λ_2 in the x-z direction. (b) show the field intensity distribution of wavelength λ_1 and wavelength λ_2 in the y-z direction.

In Fig. S11, we show the electric field distribution of λ_1 and λ_2 in different directions. For λ_1, no matter in the x-z direction or y-z direction, we find that the field intensity is concentrated in the middle of dc-Au NRs, and the field intensity is not obviously observed in the gap between the two dc-Au NRs. For λ_2, from the y-z direction, we can obviously observe that the field intensity is mainly concentrated at the gap between the two dc-Au NRs.

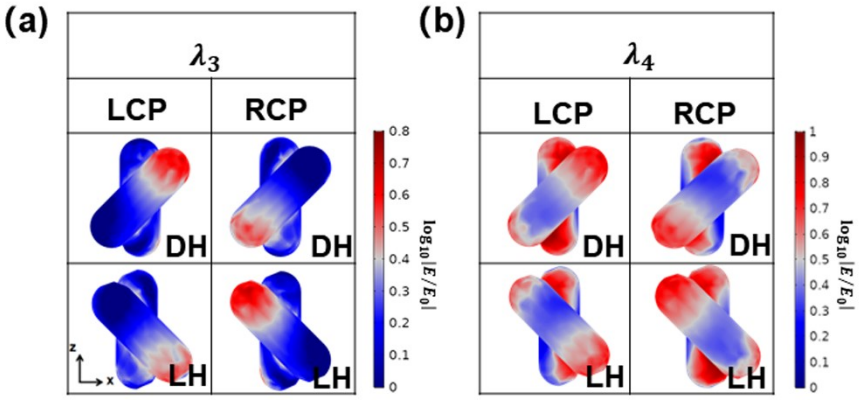

Fig. S12 Electric field enhancement distribution around the self-assembled achiral Au NRs. (a, b) show the field intensity distribution of wavelength λ_3 and wavelength λ_4 in the x-z direction.

In Fig. S12, we show the electric field distribution at wavelength $\lambda_3 = 640$ nm and $\lambda_4 = 700$ nm in the x-z direction. We find that the electric field distribution of dc-Au NRs at λ_3 and λ_4 is similar to that of Au NRs, which again confirms that they are mainly determined by extrinsic chirality.

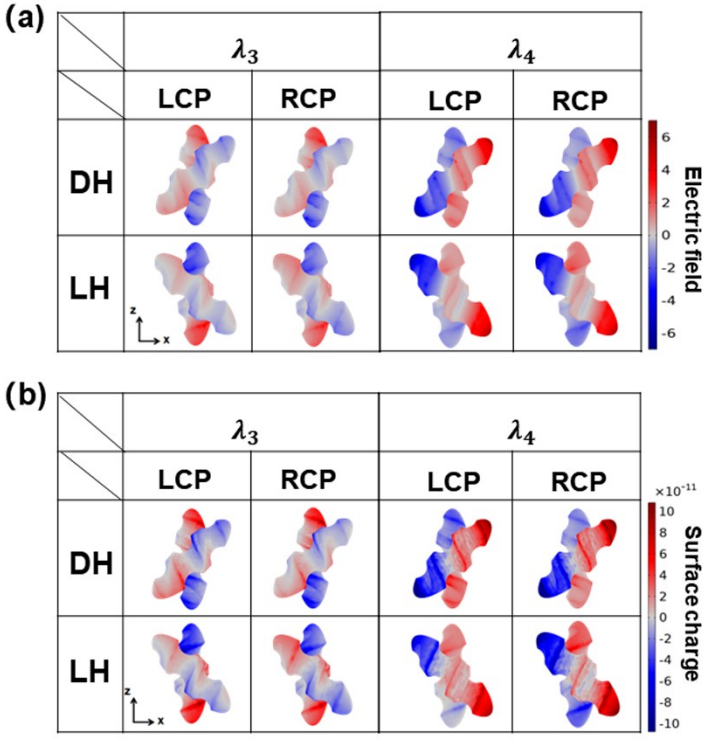

Fig. S13 Electric field distribution(a) and charge distribution(b) at wavelengths λ_3 and λ_4.

In Fig. S13, we compare the electric field distribution and the surface charge distribution of the self-assembled dc-Au NRs at λ_3 and λ_4. According to the formula $D = \varepsilon_0 E + P = \varepsilon_0 \varepsilon_r E$, $\varepsilon = \varepsilon_0 \varepsilon_r$ is the permittivity, surface charge distribution is directly proportional to the electric field distribution. Thus, we believe that both electric field distribution and charge distribution can accurately represent the bonding mode and anti-bonding mode.

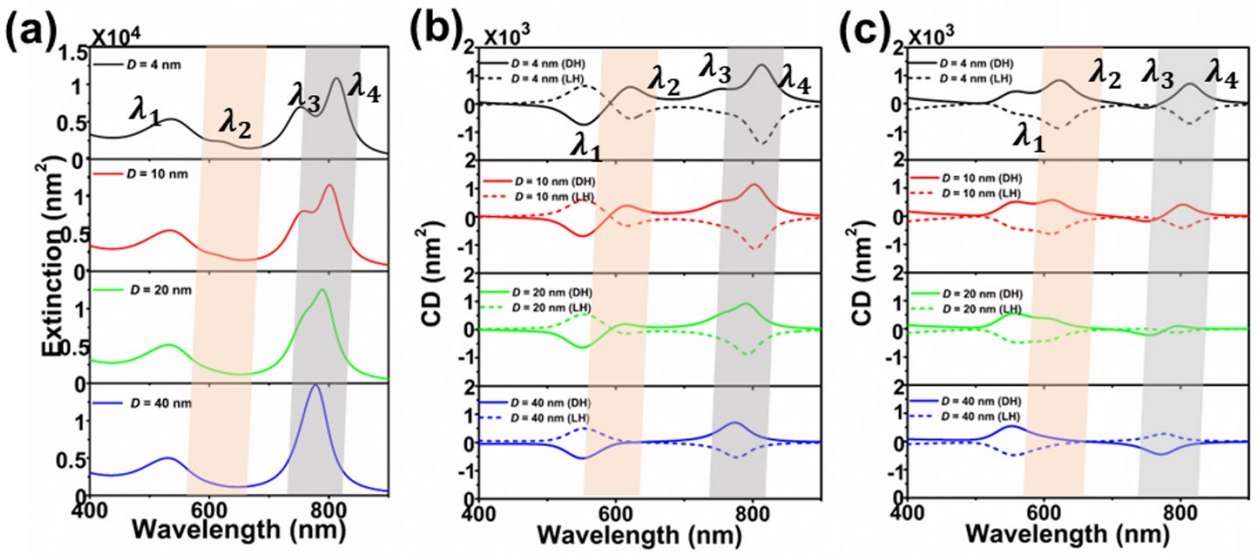

Fig. S14 Influence of separation of self-assembled dc-Au NRs on the optical response. (a, b) show the extinction spectra and PCD spectra at *D* = 4, 10, 20, and 40 nm. The solid and dashed lines represent DH/LH, which is composed of two D-Au NRs and two L-Au NRs. (c) shows the PCD spectra at *D* = 4, 10, 20, and 40 nm. The solid and dashed lines represent the DH/LH, which is composed of two L-Au NRs and two D-Au NRs. the incident light forms an angle of 0° with the long axis of the NR.

Fig. S14a and b show the extinction spectra and PCD spectra for the increasing separation *D* = 4, 10, 20, and 40 nm. It can be found that the features at λ_2 and λ_3 disappear gradually with the decrease of the spacing distance, while the feature at λ_4 blue-shifts and its intensity decreases. Fig. S14c shows the PCD spectra for *D* = 4, 10, 20, and 40 nm. The solid and dashed lines are for the DH and LH, which is composed of two L-Au NRs and two D-Au NRs. The extinction spectra are similar to Fig. S14a and is omitted here. In addition, from the PCD spectra in Fig. S14c, it can be found that no matter how the distance changes, the features at λ_1 and λ_2 have opposite sign as compared to the feature in Fig. S14b. Therefore, we speculate that the features at λ_1 and λ_2 are determined by their intrinsic chirality. The features at λ_3 and λ_4 are similar to those shown Fig. S14b, and thus we speculate that the features at λ_3 and λ_4 are determined by the extrinsic chirality.

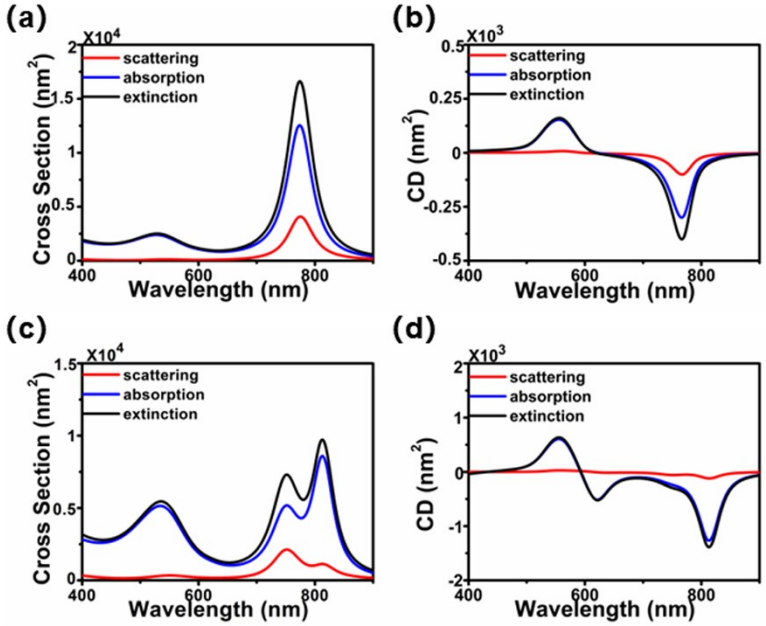

Fig. S15 Scattering (red), absorption (blue) and extinction cross section (black) (a), and the corresponding PCD (b) of dc-Au NR. Similar results (c, d) of the assembled dc-Au NRs.

In Fig. S15, we show the extinction, the absorption, and the scattering for the individual nanoparticles and the particle dimer. By comparing the results of single and dimer, we found that the absorption cross section dominates the extinction cross section in the case with both single nanoparticle and nanoparticle dimer.